Heavy-Light Mesons with Quenched Lattice NRQCD: Results on Decay Constants

A. Ali Khan[1,2] and J. Shigemitsu

The Ohio State University
Columbus, OH 43210-1106, USA

S. Collins[1,3] and C. T. H. Davies[1]

University of Glasgow,
Glasgow G12 8QQ, UK

C. Morningstar

University of California at San Diego
La Jolla, CA 92093-0319, USA

J. Sloan [3]

University of Kentucky
Lexington, KY 40506-0055, USA

---

[1]UKQCD Collaboration
[2]former address: University of Glasgow, Glasgow G12 8QQ, U.K.
[3]former address: SCRI, Florida State University, Tallahassee, FL 32306, USA

Abstract

We present a quenched lattice calculation of heavy-light meson decay constants, using non-relativistic (NRQCD) heavy quarks in the mass region of the b quark and heavier, and clover-improved light quarks. The NRQCD Hamiltonian and the heavy-light current include the corrections at first order in the expansion in the inverse heavy quark mass. We study the dependence of the decay constants on the heavy meson mass M, for light quarks with the tree level ($c_{SW} = 1$), as well as the tadpole improved clover coefficient. We compare decay constants from NRQCD with results from clover ($c_{SW} = 1$) heavy quarks.

Having calculated the current renormalisation constant Z_A in one-loop perturbation theory, we demonstrate how the heavy mass dependence of the pseudoscalar decay constants changes after renormalisation. For the first time, we quote a result for f_B from NRQCD including the full one-loop matching factors at $O(\alpha/M)$.

1 Introduction

A calculation of the decay constant of the B meson, f_B, is of interest for the determination of the unitarity triangle parameterising CP-violation in the Standard Model. The element $|V_{td}|$ of the Cabibbo-Kobayashi-Maskawa (CKM) matrix can be determined from an experimental study of $B - \overline{B}$ mixing, using f_B as one of the input parameters [1]. It can be defined through the following matrix element (in Minkowski space):

$$ip_\mu f_B = \langle 0|A_\mu|B\rangle, \tag{1}$$

where A_μ is the heavy-light axial vector current. Similarly, the vector decay constant can be defined through the relation[1]:

$$i\epsilon_\mu f_V M_V = \langle 0|V_\mu|B^*\rangle, \tag{2}$$

V_μ being the heavy-light vector current. A practical tool for calculations involving hadrons containing one heavy quark is Heavy Quark Effective Theory (HQET) [2]. It exploits the fact that in heavy-light systems, in the limit of infinite heavy quark mass m_Q, there is a spin-flavour symmetry between heavy quarks. Corrections due to finiteness of the heavy quark mass are included in an expansion in $1/m_Q$. For the decay constant one expects a heavy mass dependence of the following kind:

$$f\sqrt{M} = A_0 \left(1 + A_1/m_Q + A_2/m_Q^2 + \ldots\right). \tag{3}$$

Here, f denotes the pseudoscalar or vector decay constant and M the mass of the corresponding heavy meson. Using lattice QCD, these matrix elements can be calculated nonperturbatively from first principles. Lattice calculations of heavy-light decay constants have been performed using the relativistic 'naive' (see e.g. [3]), or the clover-improved (e.g. [4]), Wilson action for the heavy quarks. A reinterpretation of the naive relativistic action in the regime $am_Q \gtrsim 1$ has been proposed by [5]. In recent studies (e.g. [6, 7, 8, 9]), this suggestion has been implemented to various degrees. These simulations have either used heavy quarks in the mass region of the charm, relying on extrapolations to the b quark, or gone at most up to masses around the b. Lattice calculations have also been done in the infinite mass (static) limit (e.g.

---

[1]With this definition $f_V = f_B$ in the static limit

Refs. [10, 11, 12]). For a recent overview of the status of lattice calculations see Ref. [13].

Alternatively, heavy quarks can be simulated using non-relativistic QCD (NRQCD) [14], an effective theory where the operators in the action and heavy-light currents are expanded in a series in the bare inverse heavy quark mass $m_Q^{(0)}$. With this approach, one can study quarks in the whole region between the b quark and the static limit. The first calculation of heavy-light decay constants with NRQCD [15], and a following more extensive simulation [16] used an NRQCD action at $O(1/m_Q^{(0)})$ for the heavy quark and a Wilson action for the light quark; however the $O(1/m_Q^{(0)})$ corrections to the current operators were not included. A calculation using quenched configurations and Wilson light quarks that includes the current corrections is introduced in Ref. [17]. The first report on a study of decay constants where the currents are also corrected through $O(1/m_Q^{(0)})$, using Wilson light quarks and dynamical configurations, is published in [18]. In the study described in this paper, we use an NRQCD action and currents as in [18] but with quenched configurations and clover light quarks.

In Sec. 2 we explain the operators that we use in our NRQCD Hamiltonian and heavy-light currents, the simulation parameters and the interpolating operators for the mesons. The fitting procedure and results for energies and amplitudes are presented in Sec. 3. The analysis of the results follows in Sec. 4. After a brief discussion of the heavy-light meson masses using tree-level-improved ($c_{SW} = 1$), and tadpole-improved light fermions, we turn to the decay matrix elements. We compare the decay constants with tree-level-improved light quarks and NRQCD heavy quarks with results using a clover action with $c_{SW} = 1$ also for the heavy quark. This is followed by a study of axial, vector, and spin-averaged matrix elements with tree-level and tadpole-improved light clover quarks as a function of the heavy quark mass. We give results for the physical ratio f_{B_s}/f_{B_d}. Using a renormalisation constant Z_A from one-loop perturbation theory, we finally present renormalised axial matrix elements, and quote our estimate of f_B.

2 Simulation details

We choose to work in a Pauli basis where the two-component heavy quark spinor Q and the antiquark spinor $\tilde{Q}^\dagger$ decouple [18]. Only the spinor Q is

used in our simulations. The non-relativistic Lagrangian which describes the b quark is expanded through $O(1/m_Q^{(0)})$ at tree level:

$$\mathcal{L} = Q^\dagger \left(D_t + H_0 + \delta H \right) Q, \tag{4}$$

where

$$H_0 = -\frac{\Delta^{(2)}}{2m_Q^0}, \;\; \delta H = -\frac{c_B\, \vec{\sigma} \cdot \vec{B}}{2m_Q^{(0)}}. \tag{5}$$

The gauge links are tadpole improved:

$$U_\mu \to U_\mu/u_0, \;\; u_0^4 = \langle 1/3 Tr U_{\text{Plaq.}} \rangle, \tag{6}$$

so the covariant derivatives act in the following way on a Green function G:

$$\Delta_\mu G(x) = [U_\mu(x)G(x+\hat{\mu}) - U_\mu^\dagger(x-\hat{\mu})G(x-\hat{\mu})]/(2u_0); \tag{7}$$

$$\Delta_\mu^{(2)} G(x) = [U_\mu(x)G(x+\hat{\mu}) + U_\mu^\dagger(x-\hat{\mu})G(x-\hat{\mu})]/u_0 - 2G(x), \tag{8}$$

and

$$\Delta^{(2)} = \sum_\mu \Delta_\mu^{(2)}. \tag{9}$$

We use the tree level coefficient $c_B = 1$ in Eq. (5). Using tadpole-improvement, we expect that the perturbative contributions to this coefficient do not become too large. For q^* values ranging between $1/a$ and π/a, α_V lies between ~ 0.25 and ~ 0.15. The perturbative correction to this operator may thus be roughly of order 20%. The heavy quark follows the evolution equation [19]

$$G_1 = \left(1 - \frac{aH_0}{2n}\right)^n U_4^\dagger \left(1 - \frac{aH_0}{2n}\right)^n \delta_{\vec{x},0}, \; t=1, \tag{10}$$

on the first timeslice, and on the following timeslices

$$G_{t+1} = \left(1 - \frac{aH_0}{2n}\right)^n U_4^\dagger \left(1 - \frac{aH_0}{2n}\right)^n (1 - a\delta H)G_t, \; t > 1. \tag{11}$$

It has been noted [20] that this evolution equation introduces an error in principle of $O(a\Lambda_{QCD}^2/m_Q^{(0)})$ in the amplitude since the operator δH is not applied on the first timeslice. We estimated the actual size of the error by comparing it with a different evolution equation and found it to be $\sim 3 - 4\%$ for the bare lattice matrix element [21] (using clover light quarks and

4

dynamical configurations). This deviation is of the order of the statistical error (see Sec. 4), so it will be ignored here.

In the calculation of decay constants to the desired order in the $1/m_Q^{(0)}$-expansion, one has to also include the corrections to the currents. At tree level, these can be obtained by relating the heavy quark field in full QCD, h, and the nonrelativistic heavy quark field through an inverse Foldy-Wouthuysen transformation on the heavy quark spinor. At $O(1/m_Q^{(0)})$, one has:

$$h = \left(1 - iS^{(0)}\right) \begin{pmatrix} Q \\ \tilde{Q}^\dagger \end{pmatrix}, \tag{12}$$

where

$$S^{(0)} = -i\frac{\vec{\gamma} \cdot \vec{D}}{2m_Q^{(0)}}. \tag{13}$$

We write the heavy-light currents in full QCD as

$$A_\mu = \bar{q}\gamma_5\gamma_\mu h, \text{ and } V_\mu = \bar{q}\gamma_\mu h, \tag{14}$$

q being the light quark field. In the following we consider only the time component of the axial vector current and the spatial components of the vector current. In our simulations the conventions for the γ matrices are:

$$\gamma_0 = \begin{pmatrix} \mathbb{1} & 0 \\ 0 & -\mathbb{1} \end{pmatrix}, \quad \vec{\gamma} = \begin{pmatrix} 0 & i\vec{\sigma} \\ -i\vec{\sigma} & 0 \end{pmatrix}, \quad \gamma_5 = \begin{pmatrix} 0 & \mathbb{1} \\ \mathbb{1} & 0 \end{pmatrix}. \tag{15}$$

The current, corrected though $O(1/m_Q^{(0)})$, takes the form,

$$J_\mu = J_\mu^{(0)} + J_\mu^{(1)}, \tag{16}$$

where the contributions to the currents are given by:

$$J_5^{(0)} = q_{34}^\dagger Q, \quad J_5^{(1)} = -i\frac{1}{2m_Q^{(0)}}q_{12}^\dagger\vec{\sigma} \cdot \vec{D}Q \tag{17}$$

for the axial current and

$$J_k^{(0)} = -iq_{34}^\dagger\sigma_k Q, \quad J_k^{(1)} = -\frac{1}{2m_Q^{(0)}}q_{12}^\dagger\sigma_k\vec{\sigma} \cdot \vec{D}Q \tag{18}$$

for the vector current, where we use the notations q_{12} for the upper and q_{34} for the lower two components of the light quark spinor. Other operators of the same mass dimension and lattice symmetry mix under renormalisation with the Foldy-Wouthuysen operators. For the axial current, we discuss this further in subsection 4.3. A more general list of these operators can be found e.g. in Refs. [22] and [18].

We also implement the heavy quark in the static approximation, which corresponds to the Lagrangian:

$$\mathcal{L} = Q^\dagger D_t Q. \tag{19}$$

The static heavy quark propagator follows the evolution equation:

$$G_{t+1} - U_4^\dagger G_t = \delta_{x,0}. \tag{20}$$

Our light quark propagators were generated by the UKQCD Collaboration. These use a clover-improved Wilson formulation [23]. In the following we will denote our simulation with the tree level clover coefficient $c_{SW} = 1$ as Run A and the simulation with tadpole-improved clover fermions, $c_{SW} = 1/u_0^3$, with Run B. For κ values and other details of the light quarks see Table 1. The light quarks in Run A are rotated [24]:

$$
\begin{aligned}
q(x) &\rightarrow \left(1 - \frac{a}{2}\gamma \cdot D\right) q(x), \\
\overline{q}(x) &\rightarrow \overline{q}(x) \left(1 + \frac{a}{2}\gamma \cdot \overleftarrow{D}\right).
\end{aligned}
\tag{21}
$$

For the light quarks in Run B we use the normalisation $\sqrt{1 - 6\widetilde{\kappa}}$.

The clover improvement removes lattice spacing errors at $O(a)$, and we expect the remaining leading errors for light quarks at zero momentum to be $O(\alpha_s a\Lambda_{QCD})$ and $O(a^2\Lambda_{QCD}^2)$. If we use for Λ_{QCD} a value around 300 MeV ($a\Lambda_V = 0.169$ for our configurations), and $\alpha_V(1/a) = 0.247$, we estimate these errors to be $\sim 4\%$ and $\sim 3\%$ respectively.

We use quenched gauge configurations at $\beta = 6.0$ on $16^3 \times 48$ lattices, generated by the UKQCD Collaboration. The configurations were fixed to Coulomb gauge. In Table 1 we list the ensemble sizes and the lattice spacings from light spectroscopy. Degenerate pion and rho masses, lattice spacings and results for κ_{crit} and κ_s are taken for Run A from Ref. [4], and for Run B from Ref. [25]. The heavy quark parameters for both runs are given in the

6

same table. The variation of the ensemble sizes in Run B for different κ and $m_Q^{(0)}$ values between 45 and 67 is due to limited computer time. One has to note that for quenched configurations ratios of physical quantities generally differ from the corresponding ratios in the real world. Thus the values one obtains for the lattice spacing from different physical quantities are in general different. Averaging results from the $1P - 1S$ and $2S - 1S$ splitting of the Υ, one obtains $a^{-1} = 2.4(1)$ GeV at $\beta = 6.0$ [19]. Probably for heavy-light systems the appropriate lattice spacing is closer to the one determined from light hadron spectroscopy, and in the following we will use $a^{-1} = 2.0(2)$ GeV to convert lattice results into physical units. This encompasses a^{-1} from m_ρ for both runs (see Table 1) and also lattice spacings from f_π (see e.g. [26, 27]) as well as from gluonic quantities [28] at $\beta = 6.0$. The heavy quark masses $am_Q^{(0)} = 1.71$, 2.0, 2.5 are in the region of the b quark. In our later simulation (Run B) we choose one heavy mass as high as $am_Q^{(0)} = 8.0$, because in Run A with the heaviest mass being 4.0 we find it difficult to extrapolate to the static limit. The value $am_Q^{(0)} = 1.71$ corresponds to the b quark mass as determined from Υ spectroscopy with $a^{-1} = 2.4(1)$ GeV [19, 29]. If one chooses the lattice spacing from light spectroscopy, $a^{-1} \simeq 2$ GeV, $am_Q^{(0)} = 2.0$ gives approximately the same dimensionful b quark mass as the value $am_Q^{(0)} = 1.71$ used in the Υ simulations at $a^{-1} = 2.4$ GeV. This ambiguity in fixing lattice bare quark masses is typical of problems with the quenched approximation.

At the source we use the following interpolating fields for the mesons:

$$\sum_{\vec{x}_1, \vec{x}_2} Q^\dagger(\vec{x}_1)\Gamma^\dagger(\vec{x}_1 - \vec{x}_2)q(\vec{x}_2), \tag{22}$$

where $\Gamma(\vec{x}_1 - \vec{x}_2)$ factorizes into a smearing function $\phi(r = |\vec{x}_1 - \vec{x}_2|)$ and one of the 2×4 matrices in spinor space shown in table 2. We calculate heavy-light current matrix elements with the smearing function ϕ being either a delta function or a ground or excited state hydrogen-like wave function [30] at the source and a delta function at the sink, and meson correlators with all combinations of smearing functions at source and sink. For the ground state, we use

$$\phi(r) = \exp(-r/r_0), \tag{23}$$

7

	Run A		Run B	
	Light quarks			
c_{SW}	1.0		$1/u_0^3$	
rotated	yes		no	
κ values	0.1432	0.1440	0.1370	0.1381
am_π	$0.386(^{+4}_{-4})$	$0.311(^{+6}_{-5})$	$0.4137(^{+11}_{-9})$	$0.2940(^{+13}_{-12})$
am_ρ	$0.51(^{+2}_{-1})$	$0.47(^{+3}_{-2})$	$0.538(^{+3}_{-2})$	$0.463(^{+6}_{-4})$
κ_{crit}	0.14556(6)		0.13926(1)	
κ_{s}	$0.1437(^{+4}_{-5})(m_K)$		$0.13758(5)(m_K),\ 0.13726(9)(m_\phi)$	
$a^{-1}(m_\rho)$	2.0(2) GeV [4]		1.99(4) GeV [25]	
	Heavy quarks			
$am_Q^{(0)}$	1.71 2.0 2.5 4.0		1.71 2.0 4.0 8.0	
n	2 2 2 2		2 2 1 1	
	Configurations			
number	35 + time reversed		45 − 67	

Table 1: Simulation details.

$^1S_0$	$^3S_1$
$\begin{pmatrix} 0 \\ \mathbb{1} \end{pmatrix}$	$\begin{pmatrix} 0 \\ \sigma \end{pmatrix}$

Table 2: Spin operators for mesonic states.

and for the radially excited state,

$$\phi(r) = \left(\frac{1}{2}\right)^{3/2} \left(1 - \frac{r}{2r_0}\right) \exp(-r/(2r_0)), \tag{24}$$

choosing $ar_0 = 3$. The smearing is applied on the heavy quark.

3 Fitting procedure

In this section, the lattice spacing a is set to 1. On the lattice, the decay constant can be extracted from the matrix element of the local current J_k:

$$fM = \langle 0|J_k|B\rangle, \tag{25}$$

with $k = 5$ for pseudoscalar and $k = 1, 2, 3$ for vector decay constants. M denotes the meson mass. The correlation function of this current decays for sufficiently large times exponentially:

$$C_{LL}(t) \to Z_L^2 e^{-E_{\text{sim}}t} \tag{26}$$

We are using the notation C_{rs} for the correlation functions, where the index r denotes the smearing function at the source, and the index s the smearing function at the sink. L stands for a delta function, 1 for the ground state and 2 for the excited state smearing function. E_{sim} is the bare ground state binding energy and Z_L is related to the matrix element as follows:

$$Z_L = \frac{1}{\sqrt{2M}}\langle 0|J_k|B\rangle, \tag{27}$$

so that

$$f\sqrt{M} = \sqrt{2}Z_L. \tag{28}$$

To distinguish between the uncorrected current and the current containing the first order correction in the $1/m_Q^{(0)}$-expansion, we will use the definitions

$$(f\sqrt{M})^{uncorr} \equiv \frac{1}{\sqrt{M}}\langle 0|J_k^{(0)}|B\rangle, \tag{29}$$

and

$$f\sqrt{M} \equiv \frac{1}{\sqrt{M}}\langle 0|(J_k^{(0)} + J_k^{(1)})|B\rangle. \tag{30}$$

9

The current corrections we denote as

$$\delta(f\sqrt{M}) \equiv \frac{1}{\sqrt{M}} \langle 0|(J_k^{(1)}|B\rangle. \tag{31}$$

Local meson operators, however, overlap considerably with excited states with the same quantum numbers. We therefore smear the heavy quark field at the source. The amplitude of the corresponding correlation function then contains also the density Z_S, which we determine separately from smeared-smeared correlators. For sufficiently large times one has:

$$
\begin{align}
C_{11} &\rightarrow A_{11}e^{-E_{\rm sim}t}, \; A_{11} = Z_S^2, \tag{32}\\
C_{1L} &\rightarrow A_{1L}e^{-E_{\rm sim}t}, \; A_{1L} = Z_S Z_L. \tag{33}
\end{align}
$$

We extract the matrix element Z_L by fitting C_{1L} and C_{11} simultaneously to a single exponential, using a bootstrap procedure as described in [31]. Z_L is calculated as the correlated ratio $A_{1L}/\sqrt{A_{11}}$.

3.1   Run A

For $t_{min} < 5$, no single exponential fit to both C_{1L} and C_{11} is possible. After $t_{min} = 5$ the amplitudes A_{11} and A_{1L} and the ground state energy still decrease slightly, until t_{min} is moved out to 9. The dependence of results on the fit interval is shown for $m_Q^{(0)} = 4.0$ in Table 3. For $\kappa = 0.1440$ the decrease may be by more than 1σ. We use a fit interval $t_{min}/t_{max} = 9/25$ for all κ and heavy mass values. Given that the statistics are poor, we have to discard the smallest eigenvalues of the covariance matrix in the singular value decomposition (SVD) algorithm. The fit results for the amplitudes from Run A are shown in Table 4. With our limited statistics, our bootstrap procedure generates certain ensembles on which multi-exponential fits to two correlators fail, but with the original ensemble of correlation functions we can do a simultaneous fit of C_{1L} and C_{2L} to 2 exponentials. This gives a value for the ground state energy which tends to be a little higher, but in general still compatible within one standard deviation with the results fitted with just one exponential [31]. The plateau of the static correlation functions sets in around $t_{min} = 3$ and persists for about 10 timeslices, which indicates that our ground state smearing functions work well for the static case.

We determine the ratio of the axial current correction to the uncorrected axial current from a fit of the bootstrap ratio of the correlators of $\langle 0|J_5^{(0)}|B\rangle$

	$\kappa = 0.1432$			$\kappa = 0.1440$		
t_{min}/t_{max}	$E_{\rm sim}$	A_{11}	A_{1L}	$E_{\rm sim}$	A_{11}	A_{1L}
5/25	0.516(6)	211(12)	2.37(10)	0.497(6)	202(11)	2.15(11)
6/25	0.515(5)	210(11)	2.37(9)	0.495(7)	197(13)	2.11(13)
7/25	0.514(6)	210(13)	2.34(14)	0.493(8)	194(12)	2.05(14)
8/25	0.514(7)	209(15)	2.30(17)	0.491(7)	191(13)	2.00(15)
9/25	0.513(7)	210(15)	2.28(19)	0.491(8)	189(13)	1.97(16)
10/25	0.511(5)	209(14)	2.26(18)	0.489(7)	185(14)	1.91(17)

Table 3: Dependence of fit results from Run A at $m_Q^{(0)} = 4.0$ on the fit interval. All quantities are in lattice units.

		$\kappa = 0.1432$		$\kappa = 0.1440$	
C_{1L}	$m_Q^{(0)}$	A_{11}	A_{1L}	A_{11}	A_{1L}
$J_5^{(0)}$	1.71	207(8)	2.13(11)	197(8)	1.91(11)
	2.0	206(8)	2.17(10)	195(14)	1.96(15)
	2.5	212(7)	2.33(10)	193(15)	2.03(17)
	4.0	216(12)	2.59(17)	199(14)	2.27(19)
	static	222(6)	3.49(11)	219(10)	3.29(14)
$J_5^{(0)} + J_5^{(1)}$	1.71	202(16)	1.66(9)	188(18)	1.48(19)
	2.0	208(13)	1.81(10)	189(15)	1.58(11)
	2.5	210(11)	1.99(12)	188(15)	1.71(13)
	4.0	210(15)	2.28(19)	189(13)	1.97(16)
$J_k^{(0)}$	1.71	215(20)	2.02(18)	208(16)	1.83(15)
	2.0	216(7)	2.10(9)	201(9)	1.87(10)
	2.5	218(9)	2.24(13)	202(5)	1.98(10)
	4.0	226(24)	2.60(10)	209(8)	2.29(15)

Table 4: Fit results for A_{11} and A_{1L} from Run A. The columns on the left indicate the operators included in the currents.
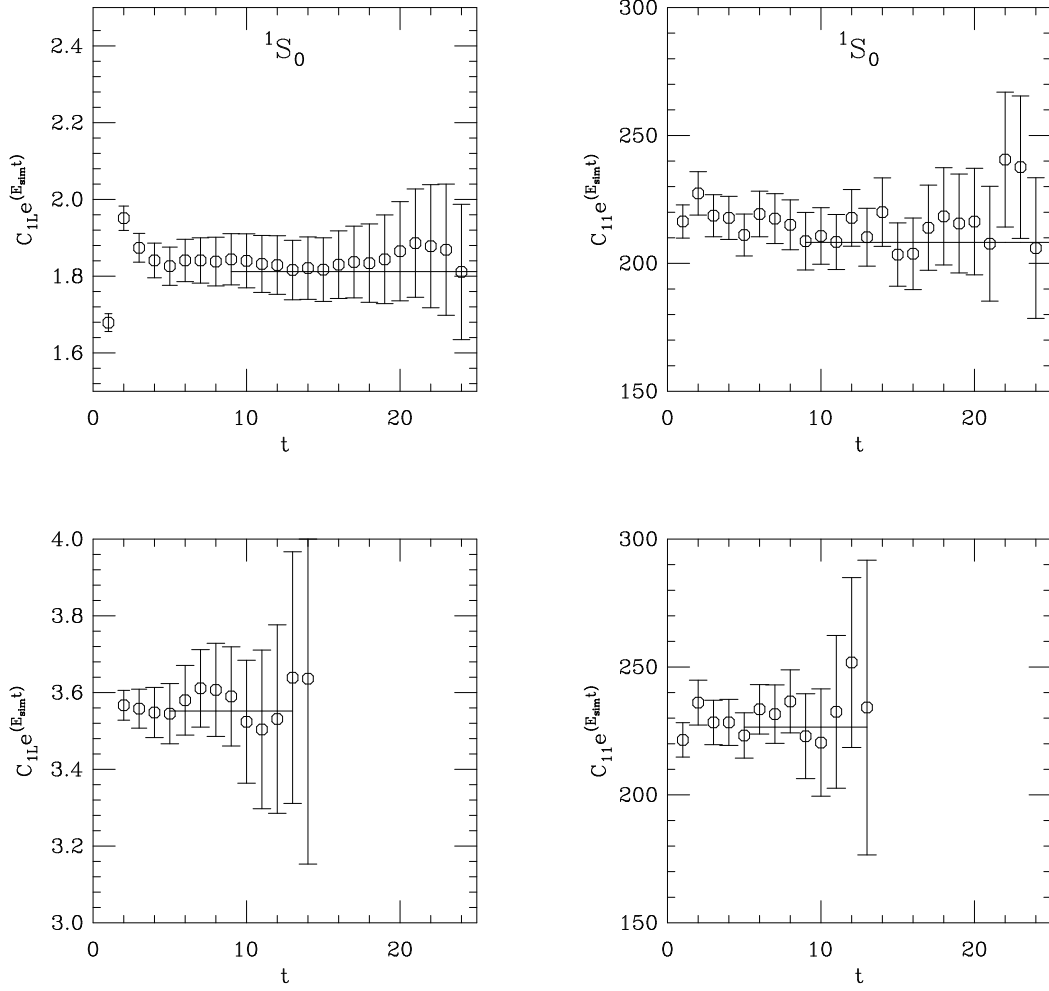
Figure 1: Effective amplitudes for smeared-local (left) and smeared-smeared correlators (right) from Run A; $\kappa = 0.1432$. The upper row shows the $^1S_0$ case at $m_Q^{(0)} = 2.0$ with the $1/m_Q^{(0)}$ correction to the current included, and the lower row, the static case. We choose the same scale of the x axis for the static correlators, to demonstrate the difference in the length of the plateau between NRQCD and static heavy quarks.

and $\langle 0|J_5^{(1)}|B\rangle$ to a constant. As fitting interval we choose $t_{min}/t_{max} = 9/25$. Results are given in Table 6.

3.2 Run B

The correlators from Run B are slightly noisier, as shown in the examples in Fig. 2. Also here we discard the lowest eigenvalues of the covariance matrix in our SVD inversions. For $\kappa = 0.1370$, we choose $t_{min} = 6$, for $\kappa = 0.1381$, $t_{min} = 5$. The upper end of the fitting window is, for $m_Q^{(0)} = 1.71$, 2.0, and 4.0, set to $t_{max} = 20$, since for larger times the signal disappears. For $m_Q^{(0)} = 8.0$, the signal disappears earlier, so we choose for $\kappa = 0.1370$, $t_{max} = 18$ and for $\kappa = 0.1381$, $t_{max} = 15$. The goodness-of-fit value Q of the fits is generally low ($Q \leq 0.1$). The fit results for the amplitudes with and without the current corrections are shown in Table 5.

At $m_Q^{(0)} = 1.71$, 2.0, and 4.0, the C_{1L} correlation functions from Run B have after $t \simeq 14$ ($\kappa = 0.1370$) or $t \simeq 12$ ($\kappa = 0.1381$) a wiggle of $\sim 1\sigma$. If we choose t_{max} for the fits not to include this wiggle, we obtain a higher Q ($\sim 0.3 - 0.4$), but the results for E_{sim} and A_{1L} are up to $\sim 2\sigma$ smaller than the values listed in Table 5. We choose to extract the decay constant using the larger fitting range. However, this variation of the result with the fit range indicates that there is a fitting uncertainty in E_{sim} and A_{1L}, associated with the choice of the fitting range, which could be for $m_Q^{(0)} = 1.71$, 2.0 and 4.0 about twice as large as the bootstrap errors. This propagates into a fitting uncertainty of $\leq 2\sigma$ for the pseudoscalar matrix elements, and of $\sim 2 - 3\sigma$ for the vector matrix element (for chirally extrapolated light quarks it is in both cases $\leq 1\sigma$). In the tables and figures, we give pure bootstrap errors on the results from Run B. We will include the fitting uncertainty where we quote our final results for decay constants (subsection 4.3). Note that the fitting uncertainty for the static case and for $m_Q^{(0)} = 8.0$ cannot be estimated in a similar way since the signal from the correlator disappears much earlier.

In a similar way to Run A, the plateau in the static correlation functions from Run B sets in slightly earlier and is clearly shorter than for the NRQCD correlators. For $\kappa = 0.1370$ we use the fit interval $t_{min}/t_{max} = 3/10$ and for $\kappa = 0.1381$, $t_{min}/t_{max} = 3/9$. Effective amplitude plots are shown in Fig. 3.

We also determine the ratio of the current corrections to the uncorrected current from the bootstrap ratio of their smeared-local correlators. For the
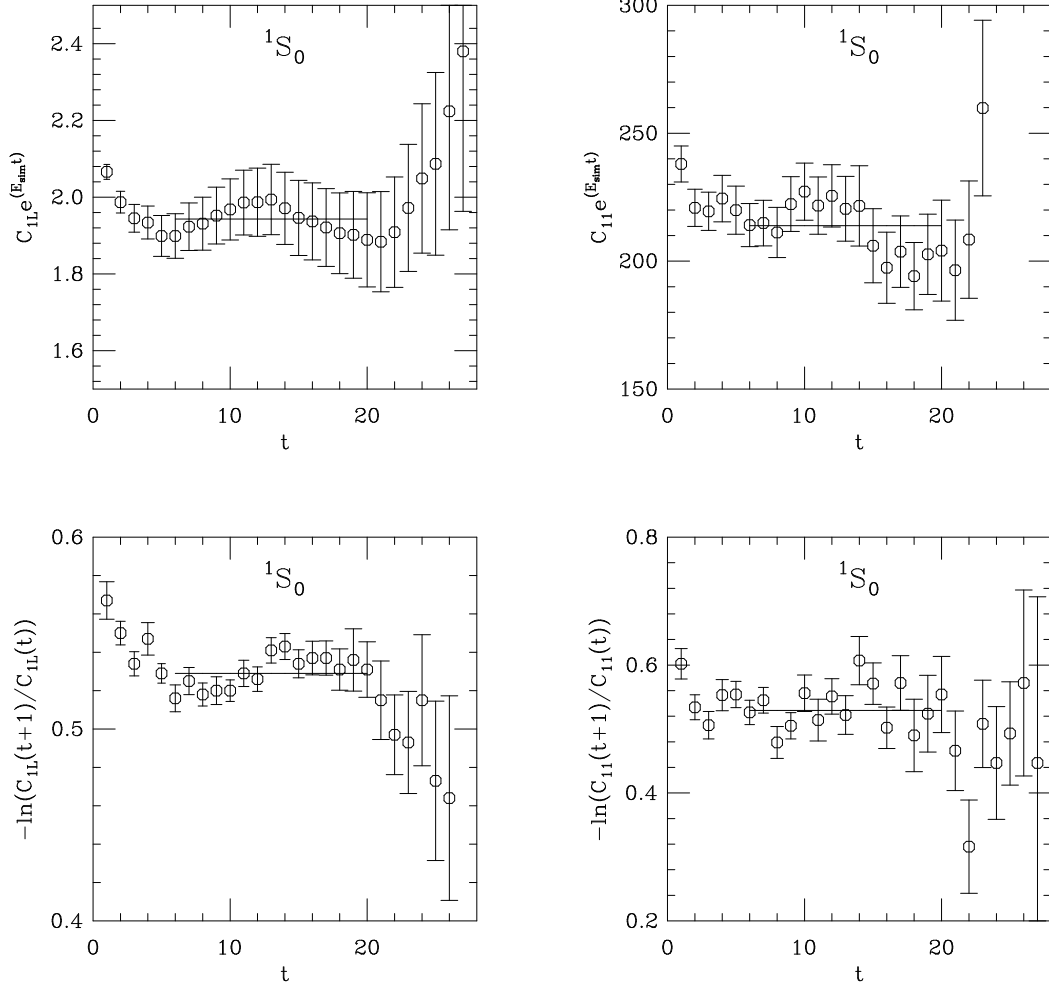
13

Figure 2: NRQCD correlators from Run B at $m_Q^{(0)} = 2.0$ and $\kappa = 0.1370$ with smeared source and local sink (left), and smeared source and sink (right). The upper row shows effective amplitudes, the lower row, effective masses. The smeared-local correlators include the $1/m_Q^{(0)}$ correction to the current.

14

C_{1L}	$m_Q^{(0)}$	$\kappa = 0.1370$			$\kappa = 0.1381$		
		E_{sim}	A_{11}	A_{1L}	E_{sim}	A_{11}	A_{1L}
$J_5^{(0)}$	1.71	0.524(4)	205(7)	2.06(7)	0.503(5)	209(7)	1.99(9)
	2.0	0.529(4)	205(6)	2.12(7)	0.503(6)	208(8)	2.02(9)
	4.0	0.540(5)	203(7)	2.32(10)	0.516(6)	213(5)	2.25(8)
	8.0	0.540(6)	204(9)	2.54(13)	0.511(8)	204(7)	2.39(11)
	static	0.540(6)	220(5)	2.98(8)	0.517(7)	213(9)	2.76(9)
$J_5^{(0)} + J_5^{(1)}$	1.71	0.525(4)	212(7)	1.84(6)	0.503(5)	210(6)	1.72(7)
	2.0	0.529(4)	214(7)	1.94(6)	0.503(6)	208(8)	1.76(7)
	4.0	0.541(5)	218(5)	2.23(8)	0.516(6)	213(6)	2.11(8)
	8.0	0.542(8)	218(8)	2.62(8)	0.513(8)	211(8)	2.37(11)
$J_k^{(0)}$	1.71	0.546(5)	218(8)	2.02(8)	0.526(7)	215(3)	1.95(9)
	2.0	0.548(5)	218(6)	2.10(7)	0.519(7)	214(5)	1.93(8)
	4.0	0.552(6)	217(7)	2.35(10)	0.524(7)	215(5)	2.19(8)
	8.0	0.550(6)	219(6)	2.62(10)	0.518(10)	216(3)	2.49(9)
$J_k^{(0)} + J_k^{(1)}$	1.71	0.544(4)	220(5)	2.14(6)	0.522(6)	216(7)	2.00(8)
	2.0	0.546(4)	220(3)	2.21(5)	0.519(6)	214(7)	2.02(8)
	4.0	0.550(5)	220(6)	2.46(9)	0.528(7)	216(4)	2.29(8)
	8.0	0.547(6)	221(5)	2.67(8)	0.518(8)	216(3)	2.51(9)

Table 5: Fit results for binding energies, A_{11} and A_{1L} from Run B. The column on the left indicates the operators contributing to the currents. All quantities are in lattice units.

ratios at $\kappa = 0.1370$ we choose the same fit intervals as described in the previous paragraph for the correlation functions. The results are shown in Table 6. The ratios at $\kappa = 0.1381$ plateau later than the correlation functions, thus we use $t_{min} = 6$ instead of 5.
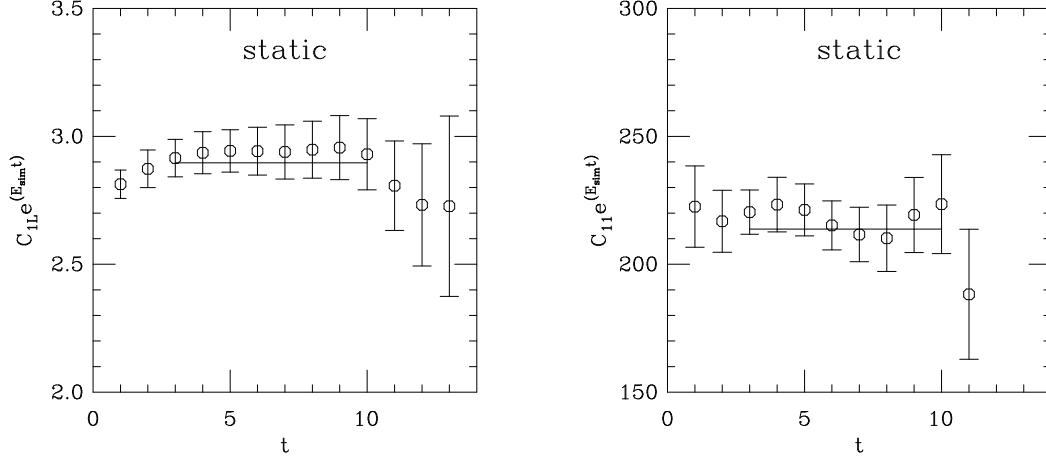

Figure 3: Static effective amplitudes from Run B at $\kappa = 0.1370$.

4 Results

We set $a = 1$ in this section, except in subsection 4.3.

4.1 Binding energies and meson masses

In NRQCD, the heavy-light meson mass differs from the exponential falloff of the meson correlators, E_{sim}, by the mass shift:

$$\Delta_{HL} = M - E_{\text{sim}}, \tag{34}$$

which depends on the renormalised heavy quark mass and the zero point of the non-relativistic heavy quark energy, E_0:

$$\Delta_{HL} = Z_m m_Q^{(0)} - E_0. \tag{35}$$

Z_m is the heavy quark mass renormalisation constant. The meson mass can be determined nonperturbatively from the ratio of finite momentum and zero

16

	Run A		Run B	
	$\kappa = 0.1432$	$\kappa = 0.1440$	$\kappa = 0.1370$	$\kappa = 0.1381$
$m_Q^{(0)}$	$\|\delta(f\sqrt{M})_{PS}/(f\sqrt{M})_{PS}^{uncorr}\|$			
1.71	0.1964(6)	0.1986(5)	0.1372(7)	0.1438(7)
2.0	0.1696(2)	0.1713(4)	0.1215(5)	0.1239(6)
2.5	0.1379(3)	0.1389(4)		
4.0	0.08800(13)	0.08863(4)	0.06561(18)	0.0672(3)
8.0			0.003368(8)	0.03447(11)
$m_Q^{(0)}$	$\|\delta(f\sqrt{M})_{V}/(f\sqrt{M})_{V}^{uncorr}\|$			
1.71			0.0455(2)	0.0468(3)
2.0			0.04032(17)	0.0410(3)
4.0			0.02178(5)	0.0223(7)
8.0			0.01118(3)	0.01151(3)

Table 6: Fit results for the ratio of the current correction to the uncorrected matrix element, in lattice units. $\delta(f\sqrt{M})_V$ has not been calculated directly in Run A.

momentum correlation functions [32]. The dispersion relation of the heavy meson is given by:

$$E_{\text{sim}}(\vec{p}) - E_{\text{sim}}(0) = \sqrt{\vec{p}^2 + M^2} - M. \tag{36}$$

We use the non-relativistic expansion of this:

$$E_{\text{sim}}(\vec{p}) = E_{\text{sim}}(0) + \frac{\vec{p}^2}{2M}, \tag{37}$$

where M is the meson mass we want to determine. In this study the errors on the finite momentum correlators are rather large and we resort to different methods to calculate the meson mass. The shift can also be determined perturbatively [33], or nonperturbatively from the mass shift Δ_{HH} (defined analogous to Δ_{HL}) in heavy-heavy systems:

$$\Delta_{HH} = 2\Delta_{HL} \tag{38}$$

In Run B, the mass shifts for $m_Q^{(0)} = 1.71$ and 2.0 are taken from the heavy-heavy results in Ref. [19], the shift for $m_Q^{(0)} = 4.0$ is from a heavy-heavy simulation which was part of this project. For $m_Q^{(0)} = 8.0$ we use perturbation theory since we expect the discretisation errors in heavy-heavy NRQCD for such large $m_Q^{(0)}$ to be large. The determination of the binding energies and the meson masses from Run A is discussed in Ref. [31].

As shown in Table 7, at κ_{crit} the pseudoscalar binding energies from Run A are $\sim 10\%$ lower than from Run B, the vector E_{sim} are $\sim 5\%$ lower and the spin averaged $\overline{E_{\text{sim}}}$, $\sim 6 - 8\%$ lower. At κ_{s}, all the binding energies are $\sim 4 - 5\%$ lower than the corresponding values from Run B. This difference corresponds to $\sim 4\sigma$. In the chirally extrapolated case error bars are larger and the difference between the two runs amounts to $2 - 3\sigma$. We expect Δ_{HL} to entirely depend on the heavy quark parameters [31], thus the difference in E_{sim} translates directly into a difference in the meson mass. The values for Δ_{HL} used in Run B and the corresponding meson masses with chirally extrapolated light quarks are given in Table 8. We note that the pseudoscalar and spin averaged masses from Run B seem to be enhanced by at least as much as the vector meson masses, which means that the enhancement of the clover term by tadpole improvement does not increase the hyperfine splitting by an amount greater than the statistical error. We came to the same conclusion when we extracted the hyperfine splitting from the ratio of the $^3S_1$

18

$m_Q^{(0)}$	κ_{crit}		$\kappa_{\text{s}}(m_K)$	
	Run A	Run B	Run A	Run B
$m_Q^{(0)}$	$E_{\text{sim}}(PS)$			
1.71	0.437(19)	0.480(12)	0.489(6)	0.513(3)
2.0	0.437(11)	0.475(13)	0.491(6)	0.515(4)
2.5	0.439(12)		0.496(7)	
4.0	0.446(15)	0.489(16)	0.499(6)	0.528(4)
8.0		0.482(16)		0.527(6)
∞	0.461(15)		0.511(6)	
$m_Q^{(0)}$	$E_{\text{sim}}(V)$			
1.71	0.464(15)	0.498(15)	0.509(6)	0.532(4)
2.0	0.463(12)	0.489(13)	0.510(6)	0.532(4)
2.5	0.464(9)		0.512(6)	
4.0	0.478(12)	0.505(15)	0.515(6)	0.539(4)
8.0		0.488(17)		0.532(6)
$m_Q^{(0)}$	$\overline{E_{\text{sim}}}$			
1.71	0.457(14)	0.493(10)	0.504(6)	0.528(3)
2.0	0.456(12)	0.486(13)	0.505(6)	0.527(4)
2.5	0.457(9)		0.508(6)	
4.0	0.462(13)	0.501(13)	0.511(6)	0.536(3)
8.0		0.487(18)		0.530(5)

Table 7: Bare ground state energies from Run A and Run B at the strange and the chirally extrapolated light quark mass, in lattice units.

$m_Q^{(0)}$	Δ_{HL}	M_{PS}
1.71	1.73(10)	2.21(11)
2.0	2.02(9)	2.50(10)
4.0	4.07(5)	4.56(7)
8.0	7.63(16)	8.11(18)

Table 8: Mass shifts used to calculate the meson masses in Run B, and chirally extrapolated meson masses using these shifts. The error on the perturbative shift at $m_Q^{(0)} = 8.0$ is an estimate of the contributions from higher orders in perturbation theory, obtained by squaring the one-loop contributions to E_0 and Z_m. All numbers are in lattice units.

and $^1S_0$ correlators (see Refs. [31, 34]). Presumably the tadpole improvement of the light fermion affects the discretisation errors in the kinetic energy and the spin-magnetic energy of the heavy quark by the same fractional amount. Since the kinetic energy is much larger than the spin-magnetic energy, the spin-independent part of E_{sim} receives the larger absolute shift due to tadpole improvement.

4.2   Bare lattice decay matrix elements

In this section we discuss the bare, unrenormalised lattice matrix elements. Renormalisation constants will be dealt with in subsection 4.3.

The $1/M$ corrections in NRQCD can be separated into contributions of the kinetic and magnetic operator in the Lagrangian and the correction to the local current:

$$f\sqrt{M} = (f\sqrt{M})^\infty \left(1 + \frac{G_{kin}}{M} + \frac{2d_M G_{hyp}}{M} + \frac{d_M G_{corr}/6}{M}\right). \qquad (39)$$

The notation is chosen to be consistent with Refs. [35, 18]. For the axial current, $d_M = 3$ and for the vector current, $d_M = -1$. With $(f\sqrt{M})^\infty$ we denote the static matrix element.

4.2.1 $f\sqrt{M}$ from Run A

Decay matrix elements in lattice units from Run A, for the pseudoscalar, vector and spin averaged cases, are shown in Table 9. To obtain an estimate of the physical matrix elements and to be able to compare with other methods, we chirally extrapolate in the light quark mass to κ_{crit} and interpolate to the strange light quark mass at κ_{s}. These extrapolations should however be used with some caution, because we only have two κ values for the light fermions. For comparison, we also list results which do not include the corrections to the current, denoted as $(f\sqrt{M})^{uncorr}$. The current corrections from Run A are given in Table 10. On the same set of configurations, the matrix elements have been calculated using clover heavy quarks ($c_{SW} = 1$) by the UKQCD Collaboration [4, 36]. Thus we are able to make a direct comparison between NRQCD and clover heavy quarks. Fig. 4 shows $(f\sqrt{M})_{PS}$ as a function of the inverse pseudoscalar meson mass M_{PS}, both for clover and NRQCD (with the current correction included) heavy quarks. Note that for the mesons with clover heavy quarks we use M_2, the 'dynamical' meson mass determined from the dispersion relation of the heavy meson [36]. The NRQCD results from Run A can be fit to a linear function in the inverse mass; a possible quadratic dependence of these results on the heavy mass cannot be resolved. The bare lattice matrix elements from both types of heavy quarks agree in the B region within errors. This is not necessarily true for the renormalised matrix elements. Renormalisation decreases $(f\sqrt{M})_{PS}$ from NRQCD in the B region by $\sim 10\%$, as detailed in subsection 4.3, whereas the current renormalisation constants have not been calculated for clover quarks with large mass.

Neither of the results presented in Fig. 4 extrapolates in the infinite mass limit to the static simulation result. Our static point agrees with UKQCD using different (Jacobi) smearing [4], and it appears that there is no sizeable excited state contamination which could artificially enhance the static result (see Table 11 and Fig. 5). Instead, the reason seems to be that the quality of the results from Run A does not allow us to predict the slope at infinite quark mass correctly. In NRQCD calculations which include larger masses and better ensembles the results do extrapolate to the static point. This is detailed in the discussion of Run B in this paper (see Fig. 7) and in Refs. [18, 21]). In these studies we find that in the region of the B there is a quadratic contribution to the slope of $f\sqrt{M}$. We do however obtain good

	$\kappa = 0.1432$	$\kappa = 0.1440$	κ_{crit}	$\kappa_{\text{s}}(m_K)$
$m_Q^{(0)}$	$(f\sqrt{M})_{PS}^{uncorr}$			
1.71	0.209(8)	0.193(8)	0.160(18)	0.199(7)
2.0	0.214(8)	0.198(9)	0.167(19)	0.205(8)
2.5	0.226(7)	0.206(10)	0.17(2)	0.214(9)
4.0	0.249(11)	0.227(13)	0.19(3)	0.235(12)
∞	0.332(7)	0.315(9)	0.281(19)	0.321(7)
$m_Q^{(0)}$	$(f\sqrt{M})_{PS}$			
1.71	0.165(7)	0.153(8)	0.128(21)	0.157(6)
2.0	0.178(7)	0.162(8)	0.132(17)	0.168(7)
2.5	0.195(7)	0.176(9)	0.138(19)	0.183(8)
4.0	0.222(13)	0.202(11)	0.163(26)	0.209(11)
$m_Q^{(0)}$	$(f\sqrt{M})_V^{uncorr}$			
1.71	0.195(10)	0.180(9)	0.15(2)	0.186(8)
2.0	0.202(7)	0.186(7)	0.155(16)	0.192(7)
2.5	0.215(9)	0.197(8)	0.161(13)	0.204(8)
4.0	0.244(8)	0.224(11)	0.185(17)	0.233(10)
$m_Q^{(0)}$	$(f\sqrt{M})_V$			
1.71	0.223(9)	0.205(9)	0.171(20)	0.212(8)
2.0	0.226(8)	0.210(9)	0.177(19)	0.216(8)
2.5	0.237(8)	0.216(11)	0.176(24)	0.224(10)
4.0	0.256(11)	0.234(13)	0.191(24)	0.242(12)
$m_Q^{(0)}$	$\overline{f\sqrt{M}}$			
1.71	0.199(9)	0.183(8)	0.153(18)	0.189(7)
2.0	0.205(6)	0.189(7)	0.158(14)	0.195(6)
2.5	0.218(8)	0.199(7)	0.163(11)	0.206(8)
4.0	0.245(8)	0.225(11)	0.185(18)	0.233(10)

Table 9: Decay matrix elements $f\sqrt{M}$ in lattice units from Run A.
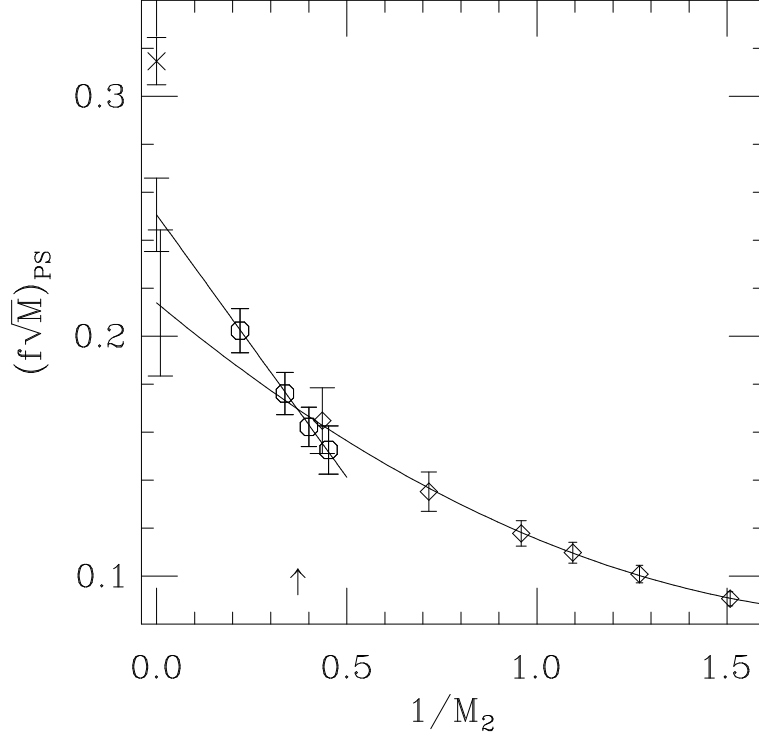
Figure 4: Unrenormalised matrix elements $(f\sqrt{M})_{PS}$ in lattice units with NRQCD heavy quarks from Run A (circles) and with tree-level clover heavy quarks (diamonds) [4, 36] at $\kappa = 0.1440$. The cross denotes the static point from Run A. The lines are correlated fits; the errors on the extrapolations to infinite mass are for clarity slightly shifted from the origin. The arrow denotes the position of the B_s meson in this plot (the light quark mass at $\kappa = 0.1440$ is close to the strange quark mass).
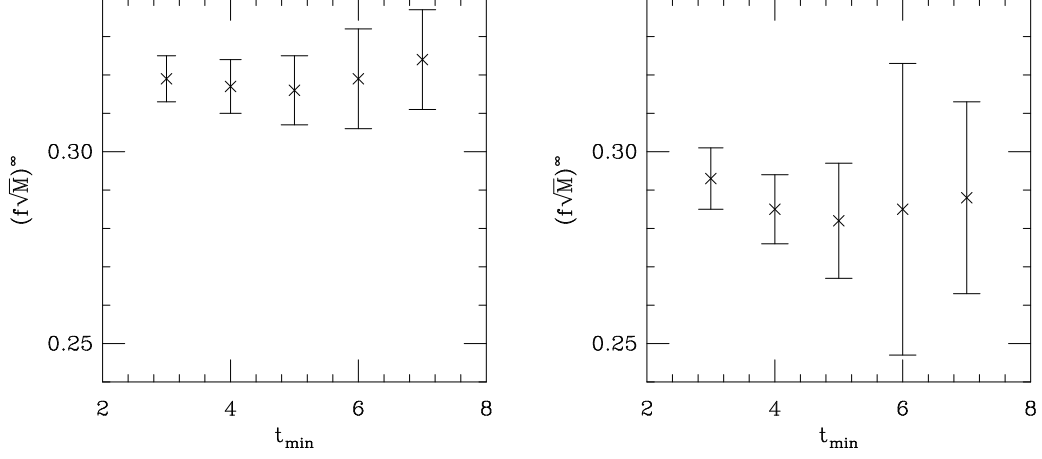
23

Figure 5: Dependence of the static matrix element from Run A, in lattice units, on the fit interval. On the left, $\kappa = 0.1440$, on the right, $\kappa = \kappa_{\mathrm{crit}}$.
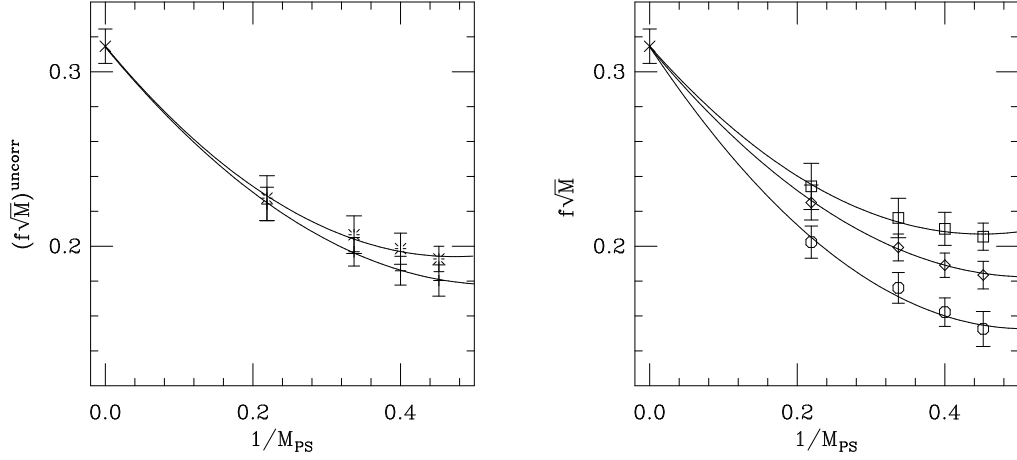

Figure 6: Unrenormalised decay matrix elements from Run A, in lattice units. On the left, pseudoscalar (bursts) and vector (pluses) matrix elements without the current correction included. On the right, pseudoscalar (circles), and vector (squares) decay constants with the current corrections. The diamonds on the right denote the spin-averaged case. The lines are correlated fits including the static point (cross). $\kappa = 0.1440$.

24

	$\kappa = 0.1432$	$\kappa = 0.1440$	κ_{crit}	$\kappa_{\text{s}}(m_K)$
$m_Q^{(0)}$			$\delta(f\sqrt{M})_{PS}$	
1.71	$-0.0412(16)$	$-0.0383(17)$	$-0.033(4)$	$-0.0394(14)$
2.0	$-0.0364(13)$	$-0.0340(15)$	$-0.029(3)$	$-0.0349(14)$
2.5	$-0.0312(10)$	$-0.0287(14)$	$-0.024(4)$	$-0.0297(13)$
4.0	$-0.0219(9)$	$-0.0202(11)$	$-0.017(2)$	$-0.0208(11)$

Table 10: Current corrections to the decay matrix elements from Run A, in lattice units.

t_{min}/t_{max}	$\kappa = 0.1432$	$\kappa = 0.1440$	κ_{crit}	κ_{s}
3/10	0.333(6)	0.319(6)	0.293(8)	0.324(5)
4/10	0.334(7)	0.317(7)	0.285(9)	0.323(7)
5/10	0.333(9)	0.316(9)	0.282(15)	0.322(8)
6/10	0.337(10)	0.319(13)	0.29(4)	0.326(11)
7/10	0.343(13)	0.324(13)	0.29(3)	0.331(14)

Table 11: The static $f\sqrt{M}$ from Run A for various fit intervals, in lattice units.

quadratic fits of the results from Run A if we include the static point into the fit. In Figure 6 we show the NRQCD and static decay matrix elements from Run A at $\kappa = 0.1440$ with a correlated fit to a quadratic function in the inverse meson mass that includes the static point. For the results without inclusion of the current corrections, at the left in Fig. 6, we find $Q = 0.94$ for the pseudoscalar and $Q = 0.96$ for the vector matrix element. The vector matrix element is smaller than the pseudoscalar matrix element. On the right, we plot the matrix elements with the correction to the current. The current correction to $(f\sqrt{M})_V$ has not been simulated in Run A, but we estimated the corrected vector current (see Table 9) using the axial current corrections in Table 9 and the relation:

$$\delta(f\sqrt{M})_V = -\frac{1}{3}\frac{\delta(f\sqrt{M})_{PS}}{(f\sqrt{M})_{PS}^{uncorr}} \cdot (f\sqrt{M})_{PS}^{uncorr}, \qquad (40)$$

which follows from Eq. (39) with the appropriate values for d_M. We find $(f\sqrt{M})_{PS}$ in the B region to be much lower, around 50%, than in the static case. The current correction gives a contribution of relative size 22 % in the B region. The spin averaged matrix element, defined as:

$$\overline{f\sqrt{M}} = \frac{1}{4}\left[(f\sqrt{M})_{PS} + 3(f\sqrt{M})_V\right],\qquad(41)$$

is also shown in Fig. 6. It can be calculated from the uncorrected matrix elements, since the current correction drops out after spin averaging (see Eq. (39)). With the current corrections included, the quadratic fit of the pseudoscalar matrix element gives $Q = 0.58$, of the vector matrix element $Q = 0.95$, and the spin averaged, $Q = 0.93$.

4.2.2 $f\sqrt{M}$ from Run B

In Fig. 7 we show the pseudoscalar, vector and spin averaged decay matrix element from Run B with correlated fits of the bare simulation results to a quadratic function in the inverse pseudoscalar meson mass. The results of these fits for the pseudoscalar matrix elements for both light κ values are shown in Table 14. Within errors, the infinite mass limit of the NRQCD matrix elements are in agreement with the static simulation result. We find the relative slope of $f\sqrt{M}$ to be of the order of 2.5 GeV. The error on the slope is however large (see Table 14), because of our small ensemble size, and the number of degrees of freedom for these fits is low. Our results from a simulation using dynamical configurations with higher statistics [21] indicate that the slope actually gets smaller with decreasing light quark mass. Renormalisation decreases the NRQCD decay matrix elements relative to the bare ones (see subsection 4.3), but their infinite mass limit is still in agreement with the (renormalised) static matrix elements.

To study the behaviour of the lattice matrix elements for the current corrections in the infinite mass limit, we perform correlated fits of $\delta(f\sqrt{M})_{PS}$ and $\delta(f\sqrt{M})_V$ as functions in the inverse pseudoscalar meson mass. Fits to a linear function have $Q \ll 1$, but fits to a quadratic function work well. The results are presented in Table 15. We find that the infinite mass limit of our results is in a reasonable agreement with zero. In Fig. 8, the axial and vector current corrections for $\kappa = 0.1370$ are shown.

From the heavy mass dependence of the spin average of the matrix elements, we can, using Eq. (39), extract the contribution of the kinetic energy
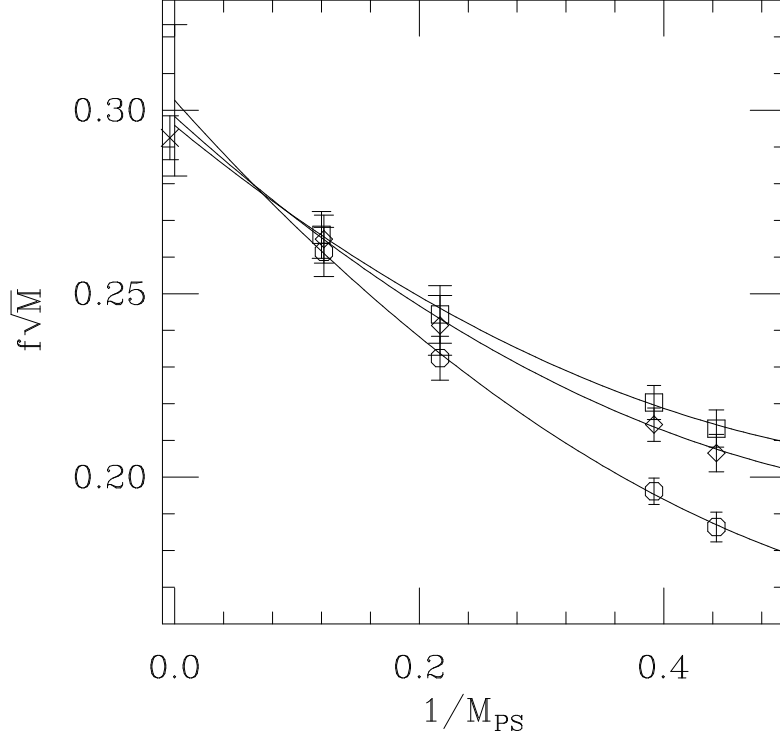
Figure 7: Unrenormalised decay matrix elements from Run B at $\kappa = 0.1370$ plotted against the inverse pseudoscalar meson mass. Circles denote $(f\sqrt{M})_{PS}$, squares $(f\sqrt{M})_V$, and diamonds the spin-averaged matrix element. Lines denote correlated fits; we indicate the error bar on the extrapolation of the pseudoscalar matrix element to infinite mass. The static point (cross) is slightly shifted from the origin for clarity. All quantities are in lattice units.
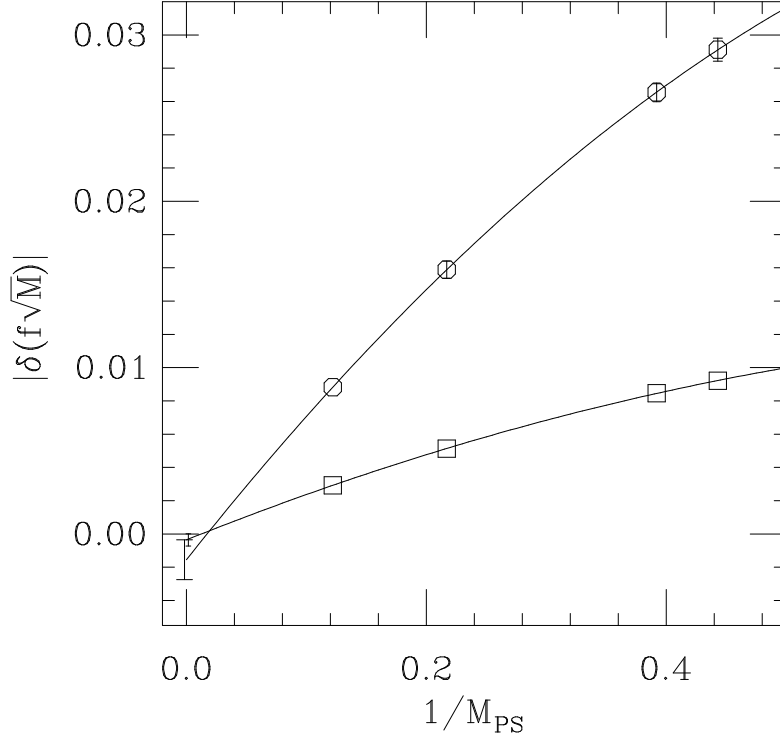
27

Figure 8: Unrenormalised current corrections from Run B, in lattice units, at $\kappa = 0.1370$, plotted against the inverse pseudoscalar meson mass. Circles denote $-\delta(f\sqrt{M})_{PS}$, and squares $\delta(f\sqrt{M})_V$. The lines denote correlated fits of $|\delta(f\sqrt{M})|$ to a quadratic function in $1/M_{PS}$. Where not shown, error bars are smaller than the symbols.

$m_Q^{(0)}$	$\kappa = 0.1370$	$\kappa = 0.1381$	κ_{crit}	$\kappa_{\text{s}}(m_K)$
$m_Q^{(0)}$	$(f\sqrt{M})_{PS}^{uncorr}$			
1.71	0.212(5)	0.201(6)	0.188(14)	0.206(4)
2.0	0.219(5)	0.203(4)	0.187(12)	0.211(3)
4.0	0.242(8)	0.225(6)	0.206(15)	0.233(4)
8.0	0.262(9)	0.243(8)	0.223(18)	0.252(6)
∞	0.293(6)	0.274(7)	0.254(15)	0.283(5)
$m_Q^{(0)}$	$(f\sqrt{M})_{PS}$			
1.71	0.186(4)	0.173(5)	0.158(12)	0.179(3)
2.0	0.196(4)	0.178(4)	0.158(9)	0.186(3)
4.0	0.232(6)	0.210(6)	0.186(14)	0.221(4)
8.0	0.261(7)	0.237(9)	0.211(17)	0.248(5)
$m_Q^{(0)}$	$(f\sqrt{M})_V^{uncorr}$			
1.71	0.202(5)	0.194(9)	0.185(18)	0.198(5)
2.0	0.210(5)	0.192(6)	0.174(12)	0.201(4)
4.0	0.236(9)	0.217(6)	0.197(16)	0.226(5)
8.0	0.261(6)	0.240(9)	0.218(19)	0.250(6)
$m_Q^{(0)}$	$(f\sqrt{M})_V$			
1.71	0.213(5)	0.198(6)	0.181(16)	0.205(4)
2.0	0.220(5)	0.200(7)	0.179(14)	0.210(4)
4.0	0.244(8)	0.226(7)	0.206(16)	0.235(5)
8.0	0.266(8)	0.243(8)	0.219(17)	0.254(6)
$m_Q^{(0)}$	$f\sqrt{M}$			
1.71	0.207(5)	0.191(5)	0.175(12)	0.199(4)
2.0	0.214(5)	0.195(6)	0.174(12)	0.204(4)
4.0	0.241(7)	0.222(7)	0.201(13)	0.231(4)
8.0	0.265(7)	0.242(10)	0.217(18)	0.253(6)

Table 12: Decay matrix elements from Run B, in lattice units.

$m_Q^{(0)}$	$\kappa = 0.1370$	$\kappa = 0.1381$	κ_{crit}	$\kappa_{\mathrm{s}}(m_K)$
$m_Q^{(0)}$	$\delta(f\sqrt{M})_{PS}$			
1.71	$-0.0291(7)$	$-0.0287(9)$	$-0.028(2)$	$-0.0289(5)$
2.0	$-0.0265(6)$	$-0.0252(6)$	$-0.0238(16)$	$-0.0258(4)$
4.0	$-0.0159(5)$	$-0.0151(4)$	$-0.0143(10)$	$-0.0155(3)$
8.0	$-0.0088(3)$	$-0.0084(3)$	$-0.0079(6)$	$-0.0086(2)$
$m_Q^{(0)}$	$\delta(f\sqrt{M})_V$			
1.71	$0.0092(2)$	$0.0091(4)$	$0.089(9)$	$0.091(3)$
2.0	$0.0085(2)$	$0.0079(2)$	$0.073(5)$	$0.0816(14)$
4.0	$0.00513(18)$	$0.00485(13)$	$0.045(4)$	$0.0498(11)$
8.0	$0.00292(7)$	$0.00277(10)$	$0.026(2)$	$0.0284(7)$

Table 13: Current corrections to the decay matrix elements from Run B, in lattice units.

κ	a_1	a_2/a_1	a_3/a_1
0.1370	0.30(2)	$-1.2(4)$	1.6(1.5)
0.1381	0.28(3)	$-1.4(7)$	2.6(2.4)

Table 14: Results of correlated fits of $(f\sqrt{M})_{PS}$ in lattice units from Run B to the function $a_1 + a_2/M_{PS} + a_3/M_{PS}^2$.

	a_1	a_2	a_3
κ	$\delta(f\sqrt{M})_{PS}$		
0.1370	$-0.0016(13)$	0.091(11)	$-0.10(4)$
0.1381	$-0.0016(14)$	0.087(14)	$-0.09(4)$
κ	$\delta(f\sqrt{M})_V$		
0.1370	$-0.0016(13)$	0.091(11)	$-0.10(4)$
0.1381	$-0.0004(5)$	0.028(5)	$-0.033(15)$

Table 15: Result of correlated fits of the current corrections from Run B to the function $a_1 + a_2/M_{PS} + a_3/M_{PS}^2$. All quantities are in lattice units.
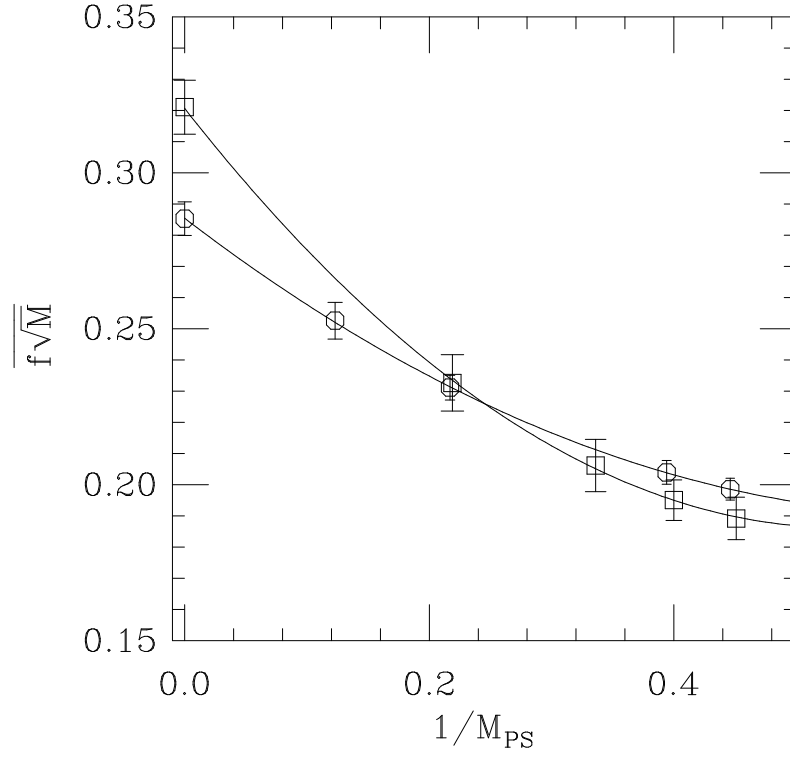
Figure 9: Spin averaged decay matrix elements, unrenormalised, in lattice units, at κ_s, plotted against the inverse pseudoscalar meson mass. Squares are results from Run A, and circles, from Run B. Lines denote correlated fits to all the points including the static.

	Run A	Run B
κ_{s}	$-1.6(2)$	$-1.05(15)$
κ_{crit}	$-2.0(5)$	$-1.2(5)$

Table 16: Results for G_{kin} from correlated fits of $\overline{(f\sqrt{M})}$ to a quadratic function in $1/M_{PS}$, in lattice units.

to $f\sqrt{M}$ [18]:

$$\overline{f\sqrt{M}} = (f\sqrt{M})^{\infty} \left(1 + \frac{G_{kin}}{M}\right). \tag{42}$$

We fit the spin-averaged matrix elements from Run A and Run B, including also the static point, to a quadratic function in $1/M_{PS}$. Results in lattice units for the strange and the chirally extrapolated light quark mass can be found in Table 16. Fig. 9 shows $\overline{f\sqrt{M}}$ at κ_{s} from both runs. For Run B, G_{kin} is found to be $\sim 2\sigma$ smaller than for Run A. However it has to be noted here that the fits include 5 points and thus there are only 2 degrees of freedom. For a definite conclusion it would be necessary to include more simulation results at heavy quark masses. Moreover, things are expected to change after inclusion of renormalisation constants. We expect the heavy mass dependence for each run to change after renormalisation in a different way. In particular, it appears that rotating the light quark in Run A with the $\gamma \cdot D$ operator introduces an additional, heavy mass dependent, contribution to Z_A and Z_V in perturbation theory.

4.2.3 $(f\sqrt{M})_{PS}/(f\sqrt{M})_V$

We can also study the behaviour of the ratios of axial and vector matrix elements in the heavy quark limit. The ratio of the matrix elements without the current correction should give an estimate for the contribution of the spin-magnetic interaction in the Hamiltonian to $f\sqrt{M}$ in Eq. (39) [18]:

$$R^{uncorr} \equiv \frac{(f\sqrt{M})_{PS}^{uncorr}}{(f\sqrt{M})_{V}^{uncorr}} \propto 1 + \frac{8G_{hyp}}{M}. \tag{43}$$

For the slope of the ratio of the matrix elements with the current correction one expects:

$$R \equiv \frac{(f\sqrt{M})_{PS}}{(f\sqrt{M})_V} \propto 1 + \frac{8G_{hyp} + 2G_{corr}/3}{M}. \tag{44}$$

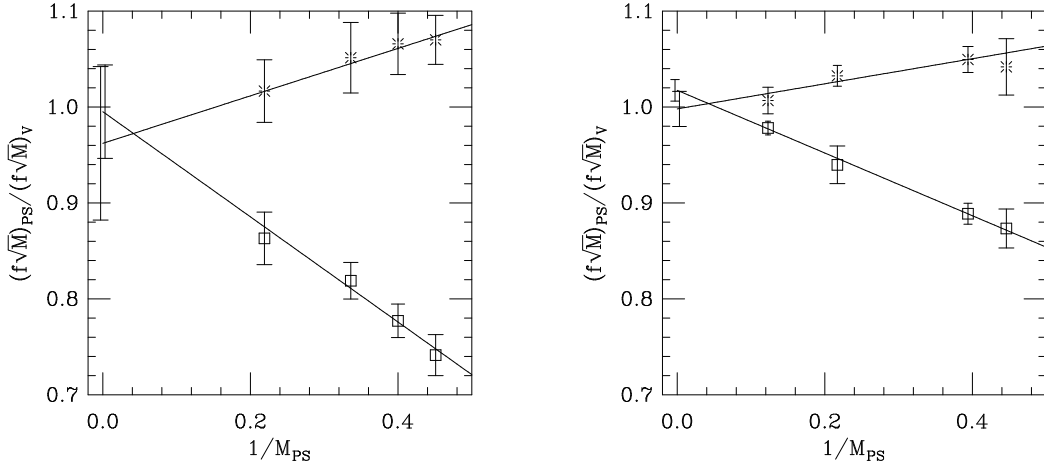The correlated ratios of axial and vector matrix elements from both runs

Figure 10: Ratio of unrenormalised axial and vector matrix elements at $\kappa = \kappa_s$ from Run A (left) and Run B (right). Bursts refer to results without the current correction included, squares to results with the current correction. The lines denote correlated fits to the ratios.

are listed in table 17. The ratios can for both runs be fit to a linear function in $1/M_{PS}$. The fit results are presented in Table 18. As expected, we find the extrapolation to the infinite mass limit to be in good agreement with one. We also perform fits with the value of the ratio fixed to one at infinite mass. In some cases these fits are slightly worse (see Table 18); however the slopes from both fit methods agree with each other. We find the slope of the uncorrected ratio and thus G_{hyp} to be slightly larger for Run A than for Run B, but the difference is not statistically significant. We note that the uncorrected ratios are independent of the light quark mass, which we also found for the $B^* - B$ hyperfine splittings [31]. The absolute value of the slope of the ratio R turns also out to be larger in Run A than in Run

33

Run A				
	$\kappa = 0.1432$	$\kappa = 0.1440$	κ_{crit}	κ_{s}
$m_Q^{(0)}$	$(f\sqrt{M})_{PS}^{uncorr}/(f\sqrt{M})_V^{uncorr}$			
1.71	1.07(5)	1.07(5)	1.07(18)	1.07(4)
2.0	1.06(4)	1.07(4)	1.09(14)	1.07(3)
2.5	1.05(3)	1.05(3)	1.05(20)	1.05(3)
4.0	1.02(3)	1.02(5)	1.02(18)	1.02(4)
$m_Q^{(0)}$	$(f\sqrt{M})_{PS}/(f\sqrt{M})_V$			
1.71	0.74(3)	0.74(3)	0.75(13)	0.74(2)
2.0	0.78(2)	0.77(3)	0.76(14)	0.78(2)
2.5	0.826(16)	0.82(3)	0.80(12)	0.82(2)
4.0	0.87(4)	0.86(4)	0.86(19)	0.86(4)
Run B				
	$\kappa = 0.1370$	$\kappa = 0.1381$	κ_{crit}	κ_{s}
$m_Q^{(0)}$	$(f\sqrt{M})_{PS}^{uncorr}/(f\sqrt{M})_V^{uncorr}$			
1.71	1.05(2)	1.04(5)	1.03(12)	1.04(3)
2.0	1.041(16)	1.057(19)	1.08(5)	1.049(12)
4.0	1.028(19)	1.036(18)	1.05(5)	1.032(13)
8.0	1.002(18)	1.010(17)	1.02(5)	1.006(13)
$m_Q^{(0)}$	$(f\sqrt{M})_{PS}/(f\sqrt{M})_V$			
1.71	0.87(2)	0.87(4)	0.88(9)	0.87(2)
2.0	0.890(14)	0.887(17)	0.88(4)	0.889(11)
4.0	0.951(14)	0.93(3)	0.90(8)	0.94(2)
8.0	0.983(9)	0.974(15)	0.96(4)	0.978(9)

Table 17: Ratio of axial and vector matrix elements from Run A and Run B, in lattice units.

Run A			Run B		
a_1	a_2	Q	a_1	a_2	Q
R^{uncorr}					
0.96(8)	0.25(19)	0.97	0.998(18)	0.13(7)	0.69
1 (fixed)	0.16(5)	0.92	1 (fixed)	0.12(3)	0.86
R					
1.0(5)	$-0.55(13)$	0.74	1.017(11)	$-0.33(5)$	0.93
1 (fixed)	$-0.56(3)$	0.90	1 (fixed)	$-0.27(2)$	0.42

Table 18: Results from correlated fits of the ratio of axial and vector decay matrix elements, in lattice units, to the function $a_1 + a_2/M_{PS}$. $\kappa = \kappa_{\mathrm{s}}$. R^{uncorr} is the ratio of the uncorrected matrix elements, R has the current corrections included.

B. Since the sign of the combination $8G_{hyp} + 2G_{corr}/3$ is opposite to G_{hyp}, this means that the current correction in Run A is considerably larger than in Run B. Another, more precise, way to determine G_{corr} is from the ratio of the current corrections to the uncorrected current [18]. From Eq (39) it follows that

$$G_{corr} = \lim_{m_Q^{(0)} \to \infty} \rho(m_Q^{(0)}) \equiv \lim_{m_Q^{(0)} \to \infty} \frac{2m_Q^{(0)} \delta(f\sqrt{M})_{PS}}{(f\sqrt{M})_{PS}^{uncorr}}. \tag{45}$$

We fit $\rho(m_Q^{(0)})$ from Run A to a linear function in $1/M_{PS}$ and find $G_{corr} = -0.739(5)$. If we include all values for ρ from Run B in a linear fit, we obtain a bad fit ($Q = 0.01$). The situation improves with a quadratic fit ($Q = 0.16$), but we obtain a better result from a linear fit, omitting the point at $m_Q^{(0)} = 4.0$ from the fit. This gives $Q = 0.44$, and for G_{corr} we obtain $-0.5703(16)$. Both fits are shown in Fig. 11. In summary, we find each of the three different $1/M$ corrections to $f\sqrt{M}$, as well as the total (compare Tables 9 and 12, and Tables 10 and 13), in Run A to be larger than in Run B.

35

	Run A		Run B	
$m_Q^{(0)}$	$\kappa = \kappa_{\mathrm{crit}}$	$\kappa = \kappa_{\mathrm{s}}$	$\kappa = \kappa_{\mathrm{crit}}$	$\kappa = \kappa_{\mathrm{s}}$
1.71	0.2030(16)	0.1978(3)	0.1494(18)	0.1403(5)
2.0	0.1747(10)	0.1707(3)	0.1265(15)	0.1227(3)
2.5	0.1410(8)	0.1385(3)		
4.0	0.08988(10)	0.0884(3)	0.0688(7)	0.06642(17)
8.0			0.0353(3)	0.03409(6)

Table 19: Ratio $|\delta(f\sqrt{M})_{PS}/(f\sqrt{M})_{PS}^{uncorr}|$ of the axial current correction to the uncorrected matrix element, in lattice units, at the chirally extrapolated and the strange quark mass.
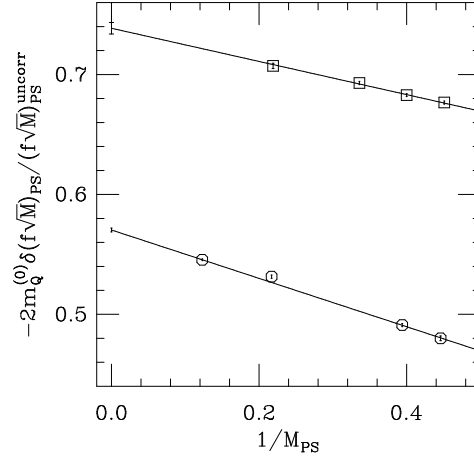
Figure 11: Ratios of unrenormalised current corrections at $\kappa = \kappa_s$ plotted as a function of the inverse heavy meson mass. Squares denote results from Run A, circles results from Run B; the lines are correlated fits to the function $a_1 + a_2/M_{PS}$.

4.2.4 f_{B_s}/f_{B_d}

The ratio f_{B_s}/f_{B_d} can be used for an extraction of the ratio of CKM matrix elements $|V_{ts}/V_{td}|$ [1]. HQET predicts that it is up to corrections $O(m_s - m_d)/m_Q$ independent of the heavy quark mass. The renormalisation constants are expected to be very weakly dependent on the light quark mass. We approximate the physical ratio f_{B_s}/f_{B_d} with the ratio of the unrenormalised lattice matrix elements:

$$\frac{f_{B_s}}{f_{B_d}} \simeq \frac{(f\sqrt{M})_{B_s}}{(f\sqrt{M})_{B_d}} \tag{46}$$

Note that the renormalisation constants used in the following subsection assume massless light quarks. The results for f_{B_s}/f_{B_d} are listed in Table 20. As expected, they are within errors independent of the heavy quark mass. We find that the ratio is larger for Run A, although not significantly. This disagreement might be a reflection of the different discretisation effects in both runs.

$m_Q^{(0)}$	Run A	Run B
1.71	1.23(18)	1.13(8)
2.0	1.26(15)	1.17(7)
2.5	1.32(12)	
4.0	1.25(25)	1.18(8)
8.0		1.17(9)
static	1.13(6)	1.10(6)

Table 20: Ratios of decay constants f_{B_s}/f_{B_d}.

4.3   Renormalised matrix elements

The results presented in the previous subsection are at tree level, i.e. they do not include the renormalisation constants which are required to match between the matrix elements in the effective theory on the lattice and the matrix elements in full QCD in the continuum.

In NRQCD, the operators that contribute to the heavy-light current mix under renormalisation. The matrix elements of the bare NRQCD current operators on the lattice, $J_{latt}^{(i)}$, the renormalised NRQCD current operators, $J_{ren}^{(i)}$, and the heavy-light current in full QCD, J_{QCD}, are thus related by:

$$\langle J_{QCD}\rangle = \sum_i \eta_i \langle J_{ren}^{(i)}\rangle = \sum_i \eta_i \sum_j Z_{ij}^{-1} \langle J_{latt}^{(j)}\rangle. \tag{47}$$

At $O(1/m_Q^{(0)})$, three operators contribute to the axial vector current:

$$J_{latt}^{(0)} = q_{34}^\dagger Q, \quad J_{latt}^{(1)} = -i\frac{1}{2m_Q^{(0)}}q_{12}^\dagger \vec{\sigma}\cdot\vec{D}Q, \quad J_{latt}^{(2)} = i\frac{1}{2m_Q^{(0)}}q_{12}^\dagger \overleftarrow{D}\cdot\vec{\sigma}Q. \tag{48}$$

$J_{latt}^{(2)}$ does not contribute at tree level. Although we did not simulate $J_{latt}^{(2)}$, we know its matrix element exactly, since translation invariance implies that at zero momentum $\langle J_{latt}^{(2)}\rangle = \langle J_{latt}^{(1)}\rangle$.

Expanding the renormalisation constants η_i and Z_{ij} through $O(\alpha)$, Eq. (47) becomes

$$
\begin{aligned}
\langle A_{QCD}^0 \rangle &= \left[1 + \alpha(B_0 - \zeta_{00} - \zeta_{10} - \frac{1}{2}(C_Q + C_q))\right]\langle J_{latt}^{(0)}\rangle \\
&+ \left[1 + \alpha(B_1 - \zeta_{01} - \zeta_{11} - \frac{1}{2}(C_Q + C_q))\right]\langle J_{latt}^{(1)}\rangle \\
&+ \left[\alpha(B_2 - \zeta_{02} - \zeta_{12})\right]\langle J_{latt}^{(2)}\rangle.
\end{aligned} \tag{49}
$$

The coefficients B_i originate from the vertex and wave function renormalisation in the continuum, the ζ_{ij} denote the vertex renormalisations on the lattice, and C_Q and C_q the heavy and the light wave function renormalisation on the lattice, respectively. α is calculated using the two-loop formula for α_V [38]. We assume a reasonable choice for the scale for α_V lies between $q^* = 1/a$ and $q^* = \pi/a$. The contribution of the rotation to the heavy-light vertex with NRQCD heavy quarks has not been calculated, so we cannot include the renormalisation constants to Run A. The renormalised matrix elements for Run B have been calculated using B_i, ζ_{ij} and C_Q from Ref. [37], and C_q from Ref. [39]. The results for chirally extrapolated and strange light quark masses are given in Table 21. Our renormalised matrix elements include an $O(\alpha a)$ discretisation correction to $\langle J_{latt}^{(0)}\rangle$. The origin of this correction and its relation to Eq. (49) will be discussed in future publications [37, 40, 42]. In Fig. 12 we compare the renormalised $a^{3/2}(f\sqrt{M})_{PS}$
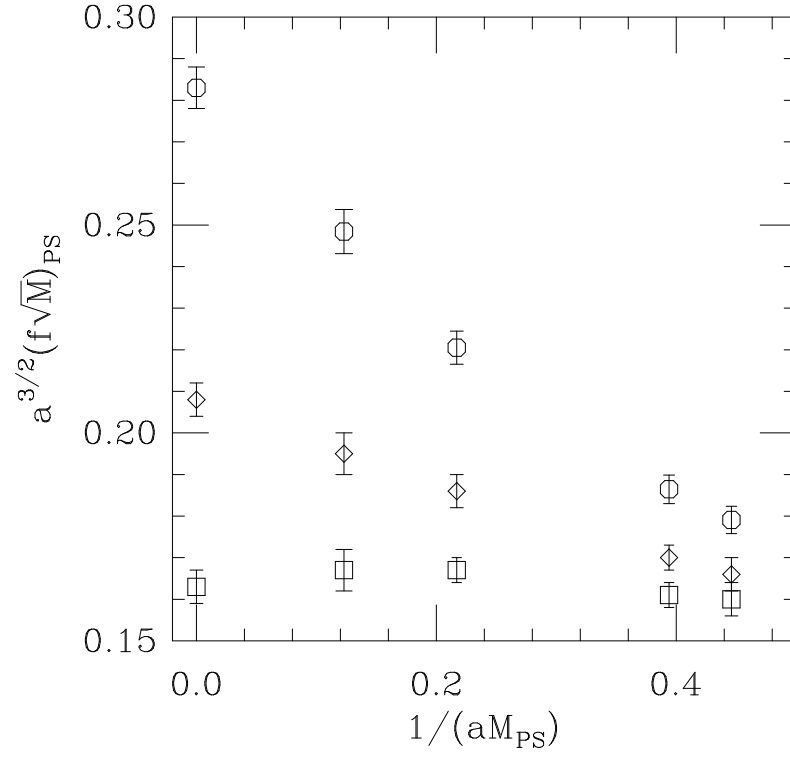
Figure 12: Matrix elements $a^{3/2}(f\sqrt{M})_{PS}$ from Run B at κ_{s}. The circles denote unrenormalised matrix elements; the squares denote renormalised results using $aq^* = 1$, and the diamonds, using $aq^* = \pi$.

$am_Q^{(0)}$	κ_{crit}		κ_{s}	
	$aq^* = 1$	$aq^* = \pi$	$aq^* = 1$	$aq^* = \pi$
1.71	0.143(14)	0.149(14)	0.160(4)	0.166(4)
2.0	0.141(11)	0.149(12)	0.161(3)	0.170(3)
4.0	0.146(13)	0.163(14)	0.167(3)	0.186(4)
8.0	0.146(15)	0.172(16)	0.167(5)	0.195(5)
∞	0.146(11)	0.186(12)	0.163(4)	0.208(4)

Table 21: Renormalised $a^{3/2}(f\sqrt{M})_{PS}$ from Run B at strange and chirally extrapolated light quark masses.

for both values of q^* with the unrenormalised matrix element. After renormalisation, the slope for large masses is remarkably smaller than before. For $aq^* = 1$, it is within errors in agreement with zero. For $aq^* = \pi$, the M dependence of the matrix elements is approximately linear, and we estimate the relative slope (the slope divided by the value at infinite mass) to be of the order of -1 GeV. The latter value is roughly in agreement with previous calculations; e.g. in Refs. [4, 6, 7] the relative slope is ~ -1 GeV. Since the results at heavy masses vary considerably depending on q^*, we do not want to make a more quantitative statement here.

For f_B, we use the result at $am_Q^{(0)} = 2.0$, the point in our simulation whose mass is closest to the actual B meson (see Table 8):

$$q^* = 1/a : \quad f_B = 0.174(28)(26)(16) \text{ GeV}$$
$$f_{B_s} = 0.198(8)(30)(17) \text{ GeV}$$
$$q^* = \pi/a : \quad f_B = 0.183(32)(28)(16) \text{ GeV}$$
$$f_{B_s} = 0.209(8)(32)(17) \text{ GeV} \tag{50}$$

This is to be compared with the tree level result, $f_B = 0.195(22)(29)(7)$ GeV, and $f_{B_s} = 0.229(8)(35)(8)$. The first error bar is the statistical error, inflated by a factor of 2 to take the fitting uncertainty of $\sim 1\sigma$ (see Sec. 3.2) into account. For f_B, the statistical error gets in addition enlarged due to the chiral extrapolation. The second error bar stems from the uncertainty in the determination of a. The third one consists of the estimated error of the perturbative calculation and due to neglected orders in the $1/M$ expansion,

and was determined as follows: The uncertainty from the choice of q^* is 5%, which can be used as an estimate of the uncertainty from higher orders in perturbation theory. Another estimate of this uncertainty, δ_2, can be obtained from the relation $\alpha^2 \delta_2 = (\alpha \delta_1)^2$, where δ_1 is the one-loop contribution. Renormalisation decreases the decay constant for q^* between π/a and $1/a$ by $9 - 10\%$ from the bare value. Squaring this yields a contribution of $\sim 1\%$ from higher orders. The numerical errors on the integrals in the perturbative calculation are estimated to be $\sim 2 - 3\%$ and propagate to the final result after being multiplied by α. Another source of error are higher order contributions in the $1/m_Q^{(0)}$ expansion. A calculation that includes also the $O(1/(m_Q^{(0)})^2)$ corrections [41, 42] indicates that these corrections are in the region of the B of the order of $\sim 3 - 4\%$. Adding this to the errors from the perturbative calculation, we quote a systematic error of 9% of the average from both q^* on our results in Eq. (50), which is represented by the third error bar. For the unrenormalised matrix elements, the third error bar consists only of the $O(1/(m_Q^{(0)})^2)$ correction. The largest errors on our results on f_B come therefore from the statistical and fitting error, which is magnified due to chiral extrapolation, and the uncertainty in a. Note that at the B, the error from the uncertainty in q^* is much smaller than for the higher masses. The quenching error is partly reflected in the error we quote for the lattice spacing. There are indications that unquenching leads to a larger value for f_B [7, 21].

For the static matrix element from Run B we obtain:

$$\begin{aligned} q^* = 1/a : \quad & f_B^\infty = 0.180(14)(27)(50) \text{ GeV} \\ q^* = \pi/a : \quad & f_B^\infty = 0.229(15)(34)(50) \text{ GeV}, \end{aligned} \tag{51}$$

while the bare result is $a^{3/2}(f\sqrt{M})^\infty = 0.254(15)$. An estimate of $aq^* = 2.18$ has been given in Ref. [43] for static heavy and Wilson light quarks. In the static case the one-loop contribution to Z_A is larger than for NRQCD around the b quark mass, thus also the variation with q^* is larger (24%). Here, the dominant error appears to originate from higher orders in perturbation theory.

For the static matrix element, the renormalisation constant has been calculated also for rotated clover fermions [44, 37]; however the $O(\alpha a)$ discretisation correction has not been determined for this case. Without this

discretisation correction, we obtain for the static f_B from Run A:

$$q^* = 1/a : \quad a^{3/2}(f\sqrt{M})^\infty = 0.154(10) \quad f_B^\infty = 0.190(12)(21) \text{ GeV}$$
$$q^* = \pi/a : \quad a^{3/2}(f\sqrt{M})^\infty = 0.202(14) \quad f_B^\infty = 0.249(17)(27) \text{ GeV}, \quad (52)$$

compared to the bare result $a^{3/2}(f\sqrt{M})^\infty = 0.281(19)$. Note also that the result in Eq. (52) is not tadpole-improved.

5 Summary and Conclusions

We report on a study of quenched heavy-light decay constants with non-relativistic heavy quarks in a mass range around the b quark and heavier. Both the NRQCD Lagrangian and heavy-light current are correct through $O(1/m_Q^{(0)})$. We performed two simulations, one uses clover light quarks with tree-level clover coefficient (Run A), the other uses tadpole-improved light quarks (Run B).

We investigated the $1/M$ behaviour of the unrenormalised decay matrix elements $f\sqrt{M}$, M being the heavy-light meson mass. In the mass region of the B meson, the correction to the static limit is large (for Run A $\sim$ 50%, for Run B $\sim 35 - 40\%$), before renormalisation constants are included. We disentangle the various $1/M$ corrections to the decay constants, and compare their size between Run A and Run B. The differences are small for the contributions of the hyperfine and kinetic term in the action, but sizeable for the current correction matrix element, at least at tree level. At the B, we find for the bare axial matrix element a difference of 18% $(1 - 2\sigma)$ for chirally extrapolated light quarks and 10% $(2 - 3\sigma)$ for strange light quarks. We expect this difference to be partly caused by a reduction of the $O(\alpha a)$ errors in Run B due to tadpole improvement. The fact that we use a rotation with a derivative operator in Run A and a normalisation with $\sqrt{1 - 6\tilde{\kappa}}$ in Run B also introduces a difference in the discretisation effects between the two runs.

We compare $f\sqrt{M}$ using NRQCD with results using clover ($c_{SW} = 1$) heavy quarks generated by UKQCD. Renormalisation constants are not included. In the region of the b quark both methods agree within errors. However, they behave quite differently at large masses, such that the clover results cannot be made to extrapolate to the static limit.

We calculated the renormalisation constant Z_A for NRQCD in one-loop perturbation theory, taking into account the mixing between the current operators. For the first time, we present renormalised pseudoscalar decay constants, and a value for f_B from NRQCD where all the matching factors through $O(\alpha/M)$ are included. The bare matrix elements show a larger slope in $1/M$ than the results from calculations with relativistic heavy quarks, but the heavy mass dependence of the renormalised matrix elements $f\sqrt{M}$ is much milder than before renormalisation.

Acknowledgements

References

[1] For reviews see for example: J. L. Rosner, in B Decays, ed. S. Stone, World Scientific (1994) 470;
M. Neubert, Int. J. Mod. Phys. A11 (1996) 4173.

[2] E. Eichten and F. Feinberg, Phys. Rev D **23** (1981) 2724;
M. Voloshin and M. Shifman, Sov. J. Nucl. Phys. **45** (1987) 292; Sov. J. Nucl. Phys. **47** (1989) 511;
H. Politzer and M. Wise, Phys. Lett. **B206** (1989) 681; Phys. Lett. B **208**(1998) 504.
N. Isgur and M. Wise, Phys. Lett. B **232** (1989) 113; Phys. Lett. B **237** (1990) 527;
B. Grinstein, Nucl. Phys. **B339** (1990) 253;
H. Georgi, Phys. Lett. **B 240** (1990) 447.

[3] C. Alexandrou *et al.*, Z. Phys. C **62** (1994) 659.

[4] UKQCD Collaboration, R. Baxter *et al.*, Phys. Rev. D **49** (1994) 1594.

[5] A. X. El-Khadra, A. S. Kronfeld and P. B. Mackenzie, Phys. Rev. D **55** (1997) 3933.

[6] T. Onogi and J. Simone, Nucl. Phys. **B** (Proc. Suppl.) **42** (1995) 434.

[7] MILC Collaboration, C. Bernard *et al.*, Nucl. Phys. **B** (Proc. Suppl.) **53** (1997) 358.

[8] JLQCD Collaboration, S. Aoki *et al.*, Nucl. Phys. **B** (Proc. Suppl.) **53** (1997) 355.

[9] APE Collaboration, C. R. Allton *et al.*, hep-lat/9703002.

[10] APE Collaboration, C. R. Allton *et al.*, Phys. Lett. B **326** (1994) 295.

[11] A. Duncan, E. Eichten, J. Flynn, B. Hill, G. Hockney and H. Thacker, Phys. Rev. D **51** (1995) 5101.

[12] UKQCD Collaboration, A. K. Ewing *et al.*, Phys. Rev. D **54** (1996) 3526.

[13] J. Flynn, Nucl. Phys. **B** (Proc. Suppl.) **53** (1997) 168.

[14] G. P. Lepage, L. Magnea, C. Nakhleh, U. Magnea and K. Hornbostel, Phys. Rev. D **46** (1992) 4052.

[15] UKQCD Collaboration, presented by C. T. H. Davies, Nucl. Phys. **B** (Proc. Suppl.) **30** (1993) 437.

[16] S. Hashimoto, Phys. Rev. D **50** (1994) 4639.

[17] T. Draper and C. McNeile, Nucl. Phys. **B** (Proc. Suppl.) 47 (1996) 429.

[18] S. Collins, U. M. Heller, J. Sloan, J. Shigemitsu, A. Ali Khan and C. T. H.Davies, Phys. Rev. D **55** (1997) 1630.

[19] C. T. H. Davies, K. Hornbostel, A. Langnau, G. P. Lepage, A. Lidsey, J. Shigemitsu and J. Sloan, Phys. Rev. D **50** (1994) 6963.

[20] T. Bhattacharya, private communication.

[21] S. Collins *et al.*, in preparation.

[22] M. Golden and B. Hill, Phys. Lett. B **254** (1991) 225.

[23] B. Sheikholeslami and R. Wohlert, Nuclear Physics **B259** (1985) 572.

[24] G. Heatlie, C. T. Sachrajda, G. Martinelli, C. Pittori and G. C. Rossi, Nucl. Phys. **B352** (1991) 266.

[25] P. Rowland, UKQCD Collaboration, private communication.

[26] C. R. Allton *et al.*, APE Collaboration, Nucl. Phys. **B413** (1994) 461.

[27] UKQCD Collaboration, presented by R. Kenway, Nucl. Phys. **B** (Proc. Suppl.) **53** (1997) 206.

[28] G. Bali and K. Schilling, Phys. Rev D **48** (1994) 2636.

[29] C. T. H. Davies *et al.* Phys. Rev. Lett. **73** (1994) 2654.

[30] C. T. H. Davies, K. Hornbostel, G. P. Lepage, A. Lidsey, J. Shigemitsu and J. Sloan, Phys. Rev. D **52** (1995) 6519.

[31] A. Ali Khan, C. T. H. Davies, S. Collins, J. Sloan and J. Shigemitsu, Phys. Rev. D **53** (1996) 6433.

[32] P. B. Mackenzie, Nucl. Phys. **B** (Proc. Suppl.) **30** (1993) 35.

[33] C. J. Morningstar, Phys. Rev D **50** (1994) 5902.

[34] A. Ali Khan, S. Collins, C .T. H. Davies, J. Shigemitsu and J. Sloan, Nucl. Phys. **B** (Proc. Suppl.) **47** (1996) 425.

[35] M. Neubert, Phys. Rev. D **46** (1992) 1076.

[36] S. Collins, PhD thesis, Edinburgh 1993, unpublished results.

[37] C. Morningstar and J. Shigemitsu, in preparation.

[38] G. P. Lepage and P. B. Mackenzie, Phys. Rev. D **48** (1993) 2250.

[39] M. Göckeler *et al.*, Nucl. Phys. **B** (Proc. Suppl.) **53** (1997) 896.

[40] J. Shigemitsu, talk given at the International Workshop "Lattice QCD on Parallel Computers", University of Tsukuba, Tsukuba, Japan, March 10–15 1997, to appear in Nucl. Phys. **B** (Proc. Suppl.).

[41] A. Ali Khan *et al.*, Nucl. Phys. **B** (Proc. Suppl.) **53** (1997) 368.

[42] A. Ali Khan *et al.*, in preparation.

[43] O. F. Hernandez and B. R. Hill, Phys. Lett. B **289** (1992) 417.

[44] A. Borrelli and C. Pittori, Nucl. Phys. **B385** (1992) 502.